Real-Time Orbit Determination of Korean Navigation Satellite System based on Multi-GNSS Precise Point Positioning

Gimin Kim[1,*], *Hyungjik* Oh[1,**], *Chandeok* Park[1,***], and *Seungmo* Seo[2,****]

[1]Department of Astronomy, Yonsei University, Seoul 03722, Republic of Korea
[2]Agency for Defense Development, Daejeon 34186, Republic of Korea

Abstract. This study proposes real-time orbit/clock determination of Korean Navigation Satellite System (KNSS), which employs the kinematic precise point positioning (PPP) solutions of multiple Global Navigation Satellite System (multi-GNSS) to compensate for receiver clock offset. Global visibility of KNSS satellites in terms of geometric coverage is first analyzed for the purpose of selecting optimal locations of KNSS monitoring stations among International GNSS Service (IGS) and Multi-GNSS Experiment (MGEX) network. While the receiver clock offset is obtained from multi-GNSS PPP clock solutions of real observation data, KNSS measurements are simulated from the dynamically propagated KNSS reference orbit and the receiver clock offset. The offset and drift of satellite clock are also generated based on two-state clock model considering atomic clock noise. Real-time orbit determination results are compared with an artificially generated true orbit, wihch show 0.4m and 0.5m of 3-dimensional root-mean-square (RMS) position errors for geostationary (GEO) and ellitically-inclined-geosynchronous-orbit (EIGSO) satellites, respectively. The overall results show that the real-time precise orbit determination of KNSS should be achievable in meter level by installing KNSS-compatible multi-GNSS receivers on the IGS and/or MGEX network. The overall process can be also used to verify integrity of KNSS monitoring stations.

1 Introduction

This study presents an alternative orbit determination (OD) of Korean Navigation Satellite System (KNSS), a regional navigation satellite system (RNSS) under development for covering Korea, in case communications with ground stations are not properly accessible. While inter-satellite ranging (ISR) was proposed for autonomous onboard orbit determination on the same environment [1, 2], the proposed algorithm uses existing GNSS infrastructure. The associated precise point positioning (PPP) techniques have been developed to find more precise navigation solutions by resolving carrier phase integer ambiguity with undifferenced observation in addition to implementing precise satellite orbit/clock data.

Introducing Multi-GNSS PPP of ground monitor stations to compensate for receiver clock bias and other metrological parameters, this paper presents experimental study of a new OD algorithm, and is organized as follows: in chapter 2, KNSS orbits are briefly introduced; in chapter 3, multi-GNSS PPP is conducted by observing from selected monitor stations of MGEX network; the overall process of KNSS OD simulation and its results are followed in chapter 4; finally, the summary and conclusion are given.

*e-mail: orion12@yonsei.ac.kr
**e-mail: jayoh@yonsei.ac.kr
***e-mail: park.chandeok@yonsei.ac.kr
****e-mail: sms@add.re.kr

2 KNSS Orbits

KNSS (Table 1) is currently composed of 4 elliptical-inclined-geosynchronous-orbits (EIGSOs) and 3 geostationary Earth orbits (GEOs) satellites. Four EIGSO satellites with different right ascension of ascending node shares the same asymmetric 8-shaped ground tracks, so that at least two EIGSO satellites are observable from Korea. Three GEO satellites are located at the longitude of 128°E, 168°E, 88°E. The ground-track repeatability of EIGSO and GEO constrains the locations of monitoring stations to a certain region. Figure 1 shows the visibility of EIGSO satellites from ground locations with respect to 4 different cutoff elevation angles. The region near the central longitude of EIGSO shows 100% visibility. As a result, the receiver in the region could observe at least 4 KNSS signals from EIGSO and GEO satellites.

3 Multi-GNSS PPP

3.1 Constellation of Monitoring Stations based on KNSS Visibility

Due to the mixed combination of EIGSO and GEO, the combination monitor stations for KNSS must be located carefully. First, to reduce the total number of stations, the stations capable of observing KNSS with greater than 5° cutoff elevation angle are selected. Then, considering visibility of GEO satellites, the ground tracks of GEO2 in

Table 1. Reference orbital elements of KNSS. Epoch is Jan 1, 2025 00:00:00.000 UTCG.

Orbital Element	GEO1	GEO2	GEO3	EIGSO1	EIGSO2	EIGSO3	EIGSO4
Semimajor axis (km)	42164	42164	42164	42164	42164	42164	42164
Eccentricity	0.000	0.000	0.000	0.075	0.075	0.075	0.075
Inclination (°)	0.000	0.000	0.000	43.0	43.0	43.0	43.0
Right Ascension of Ascending Node (°)	-	-	-	218	128	38	308
Argument of Perigee (°)	-	-	-	270	270	270	270
True Anomaly (°)	228.918	268.902	188.900	108.10	188.45	271.00	11.25

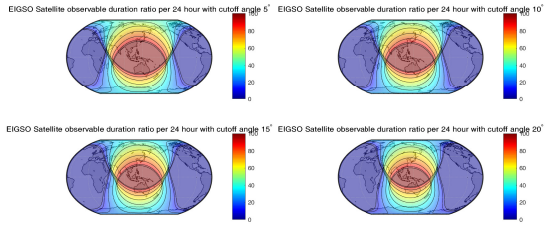

Figure 1. Global Visibility of KNSS EIGSO Satellite by the cut-off elevation angle 5°(top left), 10°(top right), 15°(bottom left) and 20°(bottom right). The contoured value shows the percentage of observable time with respect to 24 hour.

the far East and GEO3 in the far west are considered. Although these stations (No. 5, 8, 10, 12, 14 in Figure 2) barely observe the EIGSO satellites, position dilution of precision (PDOP) of the stations with respect to the GEO satellite could be improved with additional stations.

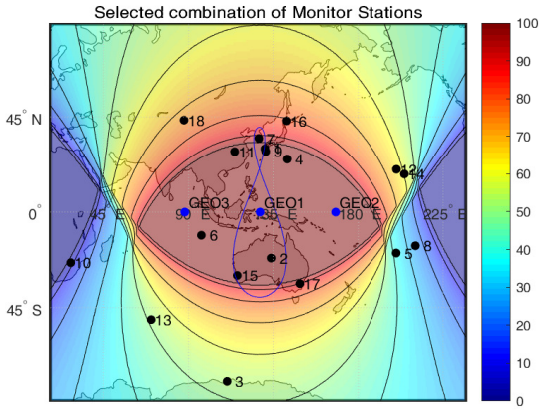

Figure 2. 18 monitor stations selected from IGS/MGEX Network. The contour and filled color represent observable duration of EIGSO in percentage when the cut-off elevation angle is set to 5°. The blue dots and blue line on the figure represent the ground-tracks of KNSS. Each number of the station corresponds to the number in Table 3.

3.2 Multi-GNSS PPP Processing

Real observation data of the stations in Figure 2 on the day of year (DoY) 1, 2018 are processed. Multi-GNSS PPP are performed by PPPH software [3] based on MATLAB. CODE solutions are used for precise GNSS satellite orbit and clock [4], and P1-C1 differential code bias (DCB) is applied. To reduce compatible measurements, code observables are smoothed by phase observables, cycle slips of which are detected by geometry-free combination on the preprocessing stage. Antenna phase offsets of satellites and receivers are corrected from IGS Antex file (IGS14.atx). Each observable is processed in adaptive Kalman filter, whose measurement weights depend on the evaluation at each update. Table 2 depicts the detailed parameters of PPP process.

Table 2. PPP filtering parameters

State	Initial Uncertainty	Process Covariance
Position	100 m	1.0 m^2/s
Receiver Clock	10^5 m	10^5 m^2/s
Trophosphere (ZTD)	0.5 m	10^{-9} m^2/s
Phase Ambiguities	2.0 m	1.0 m^2/s
System Time Difference	10.0 m	10^{-7} m^2/s

3.3 Multi-GNSS PPP Results

Table 3 shows the results of Multi-GNSS PPP using 18 stations. The position errors evaluated by comparing with CODE MGEX Final station solution show less than 10 cm overall. Up direction error shows larger than north and east direction except COCO, KOKV, TID1 and URUM station. The convergence time of PPP differs by each station, without any correlation of multi-GNSS. CKIS, GMSD, and URUM stations takes more than an hour for convergence.

Figure 3 presents a comparison between the PPP estimated receiver clock bias and CODE Clock solution. The RMS clock estimation error shows less than 20 cm for all stations. However, considering the long-term interval (5 min) of station clock product of CODE, the clock bias results cannot be analyzed.

4 KNSS Orbit Determination Simulation

4.1 Real-Time Orbit Determination Algorithm

Figure 4 shows the flowchart of KNSS simulation. Once measurements, site coordinates, antenna correction and

Table 3. PPP Results of 18 monitor stations on January 1, 2018. Letters on the third column shows GNSS availability (G: GPS, R: GLONASS, E: Galileo). The fourth and fifth column represent mean position errors and root-mean-square (RMS) position errors with respect to CODE daily final solution coordinates. N, E, and U represents North, East, and Up directions, respectively.

			Mean (cm)			RMS (cm)			
Site No.	Site	GNSS	N	E	U	N	E	U	Converg. t (minute)
1	AIRA	GR	0.0	0.7	-3.0	0.8	0.8	2.6	34.5
2	ALIC	GRE	-0.4	2.2	-2.8	1.1	4.3	4.8	12.5
3	CAS1	GRE	0.4	1.4	0.8	1.2	1.8	1.9	5.5
4	CCJ2	GR	0.2	-1.1	-3.0	0.6	1.1	4.3	50.5
5	CKIS	GRE	-0.6	-0.6	-1.3	0.7	1.6	3.5	101.5
6	COCO	GRE	-0.4	0.6	-1.6	1.0	4.6	2.2	21.0
7	DAEJ	GRE	-0.1	0.1	-3.8	1.3	0.8	3.1	18.5
8	FLRS	GR	1.4	0.3	-2.1	1.8	0.8	4.1	21.0
9	GMSD	GRE	0.3	-1.7	-3.8	0.4	1.2	3.9	82.0
10	HARB	GRE	0.1	1.3	-1.1	0.5	2.5	2.7	32.5
11	JFNG	GRE	0.0	0.4	-3.5	0.5	1.1	3.3	26.0
12	KOKV	GRE	0.5	-1.7	-2.2	0.5	3.8	2.3	13.0
13	KRGG	GRE	-0.8	1.5	0.7	0.8	-0.2	1.7	51.5
14	MKEA	GRE	0.3	-1.6	-6.1	1.1	6.5	9.2	17.5
15	PERT	GRE	-0.4	0.0	-2.5	0.8	1.1	2.5	17.0
16	STK2	GRE	-0.5	-0.7	-4.6	1.5	0.9	4.3	40.5
17	TID1	GRE	-0.8	0.5	-3.3	2.4	6.0	2.2	17.5
18	URUM	GRE	-0.7	-1.6	-1.5	0.6	2.2	1.5	89.5

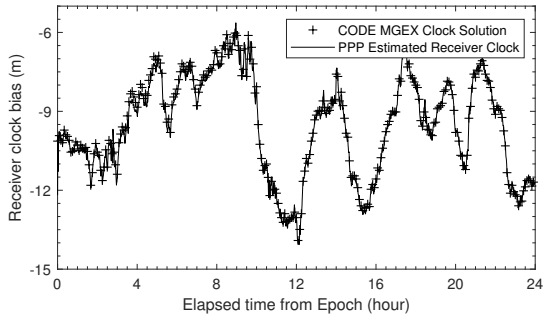

Figure 3. Estimated clock of AIRA station by PPP and 5 min-interval CODE MGEX Final Clock solution of AIRA station. The RMS errors from comparison between two clock biases show 17 cm.

station position which is known a priori are collected, measurement data is pre-processed in steps of cycle-slip detection and repair, outlier detection and carrier phase smoothing of code observable. Then, PPPH software performs PPP based on Kalman filter. The estimated receiver clock parameters and Zenith Total Delay (ZTD) are used simultaneously to make KNSS with Satellite *true* orbit and *true* clock parameters observable, where only undifferenced pseudo-range in ionosphere-free combination are used. The extended Kalman filter (EKF) is initiated with initial states as an inverse single position positioning (SPP) result in ionosphere-free code or by adding pre-defined 1 km position error for each of 3 axes when continuous SPP is unavailable. Once the filter is initialized, measurements of each station are collected, and the difference between computed or predicted measurements is obtained. In this simulation, the orbit and clock are evaluated simultaneously after state vectors are updated to confirm the orbital and clock error while running. The following assumptions apply for real-time orbit determination simulation.

- Receivers at all stations support the types of decryption and demodulation used by KNSS.
- Inter-system biases between KNSS and GPS are negligible.
- KNSS clock drift is constrained to a constant.
- Cut-off elevation angle at monitor stations is fixed to 5 deg.

4.2 Dynamic Model

The distinct characteristics of High-Earth-Orbit (HEO) satellites like EIGSO and GEO satellites justify low degree and low order aspherical geo-potential and necessitate larger third-body effects from the Sun and the Moon [10]. The atmospheric drag is negligible due to low air density in HEO. In this context, perturbations by Earth geopotential, third bodies, solar radiation pressure and relativistic dynamic correction are included in the dynamic model of KNSS satellites[equation (1)].

$$\ddot{\mathbf{r}} = \mathbf{a}_{geop} + \mathbf{a}_{body} + \mathbf{a}_{srp} + \mathbf{a}_{rel} \tag{1}$$

4.3 Clock Model

The two-state clock model [5] is implemented to generate and estimate the satellite clock bias. The clock state vector $\mathbf{x}^{clk}$ is composed of clock bias b_i (s) and clock drift d_i (s/s).

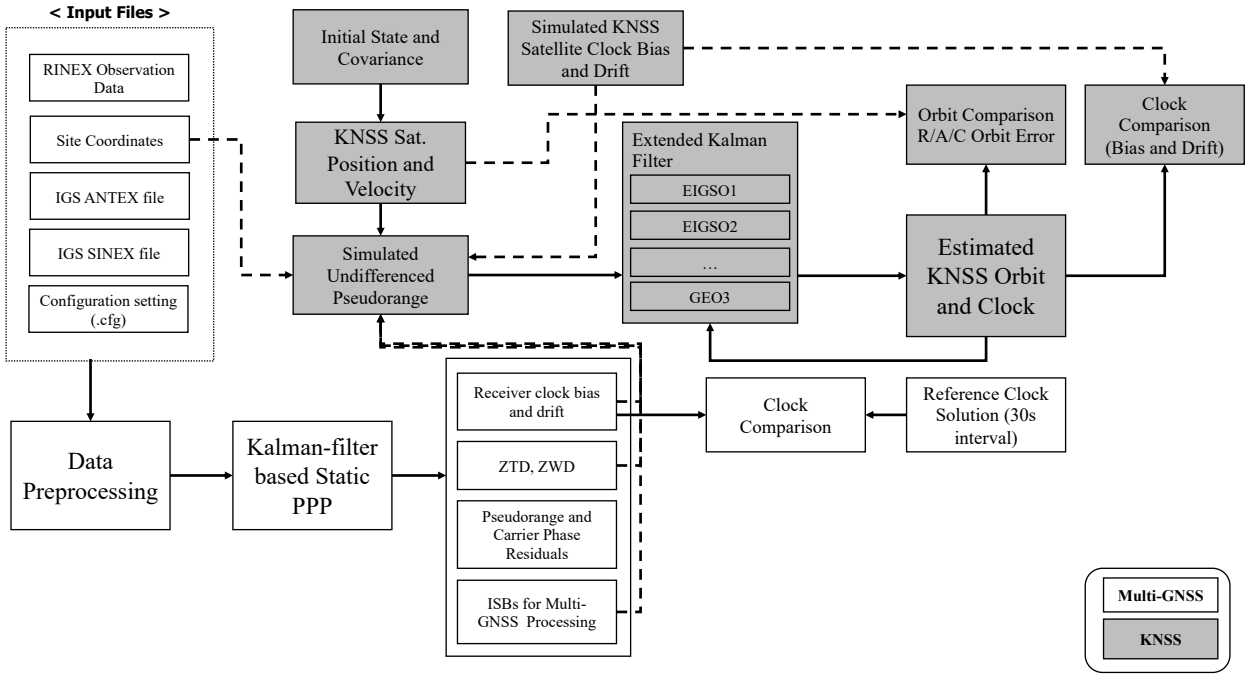

Figure 4. Flow chart representing the algorithm of KNSS OD simulation.

$$\mathbf{x}_k^{clk} = \begin{bmatrix} 1 & \tau \\ 0 & 1 \end{bmatrix} \mathbf{x}_{k-1}^{clk} + \begin{bmatrix} w_{1,k-1} \\ w_{2,k-1} \end{bmatrix}, \quad \mathbf{Q}^{clk} = \begin{bmatrix} q_1\tau + \frac{1}{3}q_2\tau^3 & \frac{1}{2}q_2\tau^2 \\ \frac{1}{2}q_2\tau^2 & q_2\tau \end{bmatrix} \tag{2}$$

Time interval τ of the above equation (2) refers to time step between adjacent epochs, which corresponds to 1 s in this study. w_1 and w_2 are defined as Gaussian random noise, with $w_1 \sim N(0, q_1)$ and $w_2 \sim N(0, q_2)$. In this clock model, the random walk frequency modulation (RWFM) of drift state results from accumulated Gaussian noise w_2, and the white frequency modulation (WFM) of bias state is due to accumulated Gaussian noise w_1. Here, q_1 and q_2 are the Allan variance of each process.

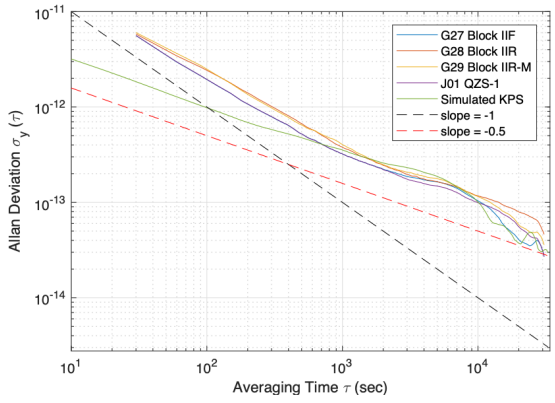

Figure 5. Allan deviation of simulated clock and other GNSS satellite clocks.

Figure 5 shows the simulated KNSS clock bias. The Allan deviations of GPS and QZSS satellite clocks are obtained by analyzing the clock bias with 30s-interval clock solutions of IGS. The Allan deviation also shows that the simulated clock bias and the drift match the real GNSS clock characteristics except the phase white noise on the $10^0 - 10^3$s averaging time. To account for these noises, additional measurement of the white noise is added to pseudorange measurement.

4.4 Condition of Simulation

Based on the PPP results, the KNSS simulation is conducted with parameters in Table 4. Fixed receiver coordinates are used for generating *true* pseudorange, while the non-stationary station position estimated from PPP is assigned to calculate the geometric distance between KNSS satellites and receiver. Measurement sampling rate is set as 1 Hz for satellite clock estimation. The estimated coordinates of monitor stations are considered as constants for 30 seconds. Consequently, KNSS measurements are modeled as the fixed station coordinates for 30 measurement updates. Receiver clock is assumed to be estimated with Gaussian random noise with 20cm of standard deviation.

5 Orbit Determination Results

5.1 Visibility

Figure 6 shows the station visibility of 6 - 14 in terms of PDOP for EIGSO satellites, which shows periodic visibility and PDOP as a result of the same ground-track characteristics. The minimum number of stations observe

Table 4. Models and parameters applied in Orbit Determination

Item	Model
Time and coordinate systems	
Time	GPS Time (GPST)
Inertial Frame	ICRF14
Earth-Fixed Frame	ITRF14
Observation model	
Pseudorange	Ionosphere-free combination
Sampling rate	1 Hz
Tropospheric delay	UNB3 with NMF [6]
Relativistic correction	Orbital eccentricity [7]
Additional Error	User Equivalent Range Error (UERE) + Receiver Clock = 0.36 m Gaussian [8]
Satellite dynamic model	
Geopotential	EGM2008 12×12 [9]
Solar radiation pressure	Spherical model+shadow function [10]
3rd-body	Moon and Sun (JPL-DE405)
Relativistic correction	Eq. of M. Correction [11]
Kalman filter setting	
Additional initial random error	1 km position error for each axes
Initial covariance (diagonal)	$[\mathbf{1}km, \mathbf{10}m/s, 5m, 10^{-3}m/s]^T$
Process noise	$10^{-6}m/\sqrt{s}, 10^{-9}m/\sqrt{s}, \mathbf{Q}_{clk}$
Measurement noise	UERE + Receiver clock

EIGSO1 satellite for 15 -17 hours from the epoch, where the maximum PDOP 10.11 occurs. Both GEO2 and GEO3 can be observed from 13 stations for 24 hours, while GEO1 can be observed from 11 stations. The PDOPs of GEO1, GEO2, and GEO3 are 7.942, 5.000 and 5.481 respectively.

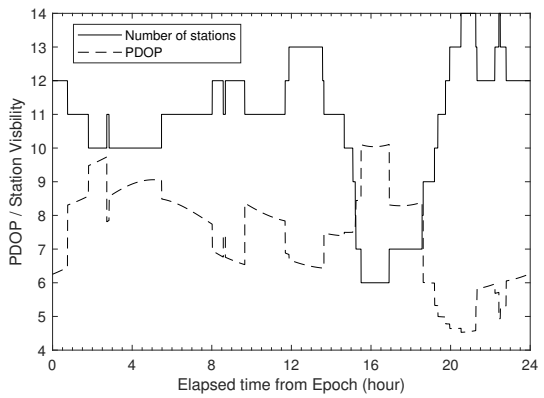

Figure 6. Station visibility of EIGSO1 with cutoff elevation angle 5°

5.2 OD Results

Orbit determination was validated by comparing the artificially generated *true* orbit and the estimated orbit from the filter. Table 5 shows the root-mean-square (RMS) of radial, along-track, cross-track, and 3-dimensional position errors of each KNSS satellite. RMS values are evaluated from about 2 hours after the epoch to the end of the day. It can be seen that the radial direction error is the most critical. Meanwhile, the orbit propagation originated from insufficient measurement did not occur by continuous visibility of more than 11 stations.

Table 5. Orbit determination RMS error

Satellite	Radial (m)	Along-track (m)	Cross-track (m)	3D (m)
EISGO1	0.422	0.041	0.039	0.426
EIGSO2	0.398	0.039	0.046	0.403
EIGSO3	0.282	0.045	0.041	0.289
EIGSO4	0.364	0.044	0.040	0.369
GEO1	0.372	0.041	0.032	0.375
GEO2	0.462	0.034	0.037	0.465
GEO3	0.369	0.038	0.029	0.372

5.3 Clock Estimation Results

Clock determination is validated by comparing the *true* clock and the estimated clock. Table 6 shows the root-mean-square (RMS) of clock bias estimation error of each satellite. The assumption of the PPP-residual receiver clock bias treated as Gaussian error does not correspond to the real clock. Therefore, the remaining systematic bias must be modeled more precisely to decrease the clock bias estimation error.

Table 6. Clock determination RMS error

Satellite	Clock bias (m)	Clock bias (ns)
EISGO1	0.420	1.401
EIGSO2	0.396	1.321
EIGSO3	0.281	0.939
EIGSO4	0.362	1.209
GEO1	0.369	1.231
GEO2	0.458	1.529
GEO3	0.366	1.222

6 Summary and Conclusion

An alternative real-time orbit determination of Korean Navigation Satellite System was proposed. The algorithm uses the KNSS navigation signal while users only have inaccurate KNSS clock or ephemeris. Adapting the multi-GNSS PPP for high precision receiver position and clock

estimation, KNSS orbit as well as its clock has been successfully and precisely determined within 1 meter-level accuracy in simulation environment. Meanwhile, long-term stability of multi-GNSS PPP solution will remain as further work.

7 Acknowledgement

This study is conducted as a research part of national GNSS research center which is supported by agency for defense development (ADD) and defense acquisition program administration (DAPA).

References

[1] J. Choi, H. Oh, C. Park, S.Y. Park, International Journal of Aeronautical and Space Sciences, **18**,2, 327-333 (2017)

[2] K. Shin, H. Oh, S.Y. Park, C. Park, Journal of Astronomy and Space Sciences, **33**,1, 37-44, (2016)

[3] Bahadur, B., Nohutcu, M.,GPS Solutions, 22, 4, 113 (2018)

[4] L.Prange, R. Dach, S. Lutz, S. Schaer, A. Jäggi, *IAG 150 Years* (Springer, Cham, 2015) 767-773.

[5] L. Galleani, Metrologia **45**, 6, S175 (2008)

[6] R. Leandro, M.C. Santos, R.B. Langley, In Proceedings of ION NTM, **52**, 1, 564-73, (2006)

[7] N. Ashby, Living Reviews in relativity, **6(1)**,1 (2003)

[8] E.D. Kaplan, C. Hegarty, eds., *Understanding GPS/GNSS: principles and applications* (Artech House, 2017)

[9] N.K. Pavlis, S.A. Holmes, S.C. Kenyon, J.K. Factor, Journal of Geophysical Research: Solid Earth, **117**, B4 (2012)

[10] O. Montenbruck, and E. Gill, *Satellite orbits: models, methods and applications* (Springer Science & Business Media , 2012)

[11] G. Petit, B. Luzum, *IERS conventions (2010)* (Bureau international des poids et mesures, France, IERS-TN-36. 2010)